International Journal of Nanomedicine

Dovepress
open access to scientific and medical research

Open Access Full Text Article

ORIGINAL RESEARCH

^{131}I-Labeled Multifunctional Polyethylenimine/Doxorubicin Complexes with pH-Controlled Cellular Uptake Property for Enhanced SPECT Imaging and Chemo/Radiotherapy of Tumors

Jingyi Zhu[1,*]
Junxing Yang[2,*]
Lingzhou Zhao[3,*]
Pingping Zhao[1]
Jiqin Yang[4]
Jinhua Zhao[3]
Wenjun Miao[1]

[1]School of Pharmaceutical Sciences, Nanjing Tech University, Nanjing, 211816, People's Republic of China; [2]College of Biotechnology and Pharmaceutical Engineering, Nanjing Tech University, Nanjing, 211816, People's Republic of China; [3]Department of Nuclear Medicine, Shanghai General Hospital, Shanghai Jiao Tong University School of Medicine, Shanghai, 200080, People's Republic of China; [4]Department of Nuclear Medicine, General Hospital of Ningxia Medical University, Yinchuan, Ningxia, 750004, People's Republic of China

*These authors contributed equally to this work

Correspondence: Jinhua Zhao
Department of Nuclear Medicine, Shanghai General Hospital, Shanghai Jiao Tong University School of Medicine, Shanghai, 200080, People's Republic of China
Tel +86 21 3779 8352
Fax +86 21 3779 8352
Email zhaojinhua1963@126.com

Wenjun Miao
School of Pharmaceutical Sciences, Nanjing Tech University, Nanjing, 211816, People's Republic of China
Tel +86 25 5813 9942
Fax +86 25 5813994
Email miaowj@njtech.edu.cn

Introduction: Smart theranostic nanosystems own a favorable potential to improve internalization within tumor while avoiding nonspecific interaction with normal tissues. However, development of this type of theranostic nanosystems is still a challenge.

Methods: In this study, we developed the iodine-131 (^{131}I)-labeled multifunctional polyethylenimine (PEI)/doxorubicin (DOX) complexes with pH-controlled cellular uptake property for enhanced single-photon emission computed tomography (SPECT) imaging and chemo/radiotherapy of tumors. Alkoxyphenyl acylsulfonamide (APAS), a typical functional group that could achieve improved cellular uptake of its modified nanoparticles, was utilized to conjugate onto the functional PEI pre-modified with polyethylene glycol (PEG) with terminal groups of monomethyl ether and N-hydroxysuccinimide (mPEG-NHS), PEG with terminal groups of maleimide and succinimidyl valerate (MAL-PEG-SVA) through sulfydryl of APAS and MAL moiety of MAL-PEG-SVA. This was followed by conjugation with 3-(4'-hydroxyphenyl)propionic acid-OSu (HPAO), acetylating leftover amines of PEI, complexing DOX and labeling ^{131}I to generate the theranostic nanosystems.

Results: The synthesized theranostic nanosystems exhibit favorable water solubility and stability. Every functional PEI can complex approximately 12.4 DOX, which could sustainably release of DOX following a pH-dependent manner. Remarkably, due to the surface modification of APAS, the constructed theranostic nanosystems own the capacity to achieve pH-responsive charge conversion and further lead to improved cellular uptake in cancer cells under slightly acidic condition. Above all, based on the coexistence of DOX and radioactive ^{131}I in the single nanosystem, the synthesized nanohybrid system could afford enhanced SPECT imaging and chemo/radioactive combination therapy of cancer cells in vitro and xenografted tumor model in vivo.

Discussion: The developed smart nanohybrid system provides a novel strategy to improve the tumor theranostic efficiency and may be applied for different types of cancer.

Keywords: polyethylenimine, pH-controlled cellular uptake, doxorubicin, iodine-131, SPECT imaging, chemo/radiotherapy

Introduction

Currently, nanoparticle technologies play an important role in cancer therapy, especially to build various intelligent drug delivery systems for efficient cancer therapy.[1–9] More advanced strategies aim to incorporate diagnostic and therapeutic agents into one nanosystem for imaging guided cancer treatment to overcome the

Received: 22 March 2021
Accepted: 8 July 2021
Published: 30 July 2021

deficiencies of clinical cancer therapy.[10–17] Based on the advanced nanoscience and nanotechnology, numerous theranostic nanosystems have been promoted, such as graphene oxide,[18,19] single-walled carbon nanotubes,[20,21] liposomes,[22,23] micelles,[24,25] dendrimers,[26,27] and metal-based photothermal nanomaterials.[28,29] The developed theranostic nanosystems own the great potential to improve the pharmacokinetics, pharmacology, biomedical performance, and bioavailability of imaging agents and therapeutic agents for superior cancer therapy in vivo.[30,31] Although the created theranostic nanoparticles (NPs) exhibit certain therapeutic efficiency and real-time imaging effect towards tumor, the theranostic efficiency is also influenced by the relatively low imaging signal and inadequate drug dosage, which is ascribed to the relatively low accumulation of NPs at tumor site via circulation in vivo. Therefore, optimizing the functions of theranostic nanosystems to improve their internalization within tumor while avoiding nonspecific interaction with normal tissues is the favorable strategy to be advocated.

According to the microenvironment difference between tumor and normal tissues, many smart nanocomposites were created with functions to respond to tumor microenvironment to achieve selective tumor accumulation.[26,32–35] Among numerous functional groups, a sort of pH-responsive charge conversional coating moiety is attractive due to its high sensitivity to tumor pH condition, which could achieve pH-controlled cellular uptake under tumor microenvironment. As a typical representative, alkoxyphenyl acylsulfonamide (APAS) enables surface charge switchable (from neutral to positive) with a decrease in pH (from 7.4 to 5.5).[36,37] With the surface coating of APAS, the generated NPs exhibit neutral at physiological pH (pH 7.4) and switch to be positively charged at tumor pH (pH 6.0), which mediate the improved cellular uptake in cancer cells according to the electrostatic binding between the particle surface and cell membrane.[36] Mizuhara et al utilized APAS to decorate gold (Au) NPs to realize enhanced cellular uptake (45 ng/well) at tumor pH.[36]

As a sort of highly branched, monodispersed polymer, hyperbranched polyethylenimine (PEI) is able to be utilized as a superior nanoplatform to build theranostic nanosystem on account of its low-cost preparation, solubility, chemical stability, facile surface functionalization and NPs loading property in the field of chemistry, materials, and biological science.[38–42] Based on the precise structure and prominent physicochemical properties, numerous PEI-based theranostic nanosystems for tumor biomedical imaging and therapy have been established.[43–45] For instance, Luo et al have developed folic acid (FA) and disulfide polyethylene glycol (SS-PEG) modified PEI with complexing of superparamagnetic iron oxide nanoparticles (SPIONs) as a small interfering RNA (siRNA) delivery system for targeted gene therapy and magnetic resonance (MR) diagnosis of gastric cancer.[46] Zhao et al have synthesized glioma-specific peptide chlorotoxin (CTX)-conjugated PEI-entrapped Au NPs (Au PNPs) with radionuclide iodine-131 (^{131}I) labeling for single-photon emission computed tomography (SPECT)/computed tomography (CT) imaging and radiotherapy of glioma.[44] Gao et al have constructed a nanocomposite fluorescent probe via electrostatic assembly of PEI-linked carbon dots and hyaluronic acid-modified doxorubicin (DOX) for fluorescence imaging-guided chemotherapy of CD44-overexpressed HeLa cells.[47] Overall, a comprehensive research investigation indicates PEI could be utilized as favorable nanoplatform to build theranostic nanosystem and own tremendous potential to improve its performance via functionalization for enhanced theranostic application.

Inspired by the characteristics of APAS and our previous successes in the creation of radionuclide-labeled PEI nanosystems for multi-mode imaging application, here we attempted to establish a smart ^{131}I-labeled multifunctional PEI/DOX complexes with pH-controlled cellular uptake function for enhanced SPECT imaging and chemo/radioactive combination therapy of tumors. In this research, PEI was first sequential conjugated with polyethylene glycol (PEG) with terminal groups of monomethyl ether and N-hydroxysuccinimide (mPEG-NHS), PEG with terminal groups of maleimide and succinimidyl valerate (MAL-PEG-SVA), APAS, and 3-(4'-hydroxyphenyl)propionic acid-OSu (HPAO) to generate multifunctional PEI (PNPs), followed by acetylating leftover amines of PEI, complexing DOX and labeling ^{131}I to create the theranostic nanosystems APAS-^{131}I-PNPs/DOX complexes (Scheme 1). The final APAS-^{131}I-PNPs/DOX complexes were characterized using a variety of techniques. The solubility, release kinetics, and pH-responsive charge conversion efficiency of APAS-PNPs/DOX complexes without ^{131}I labeling were thoroughly evaluated. The specific cellular uptake of APAS-PNPs/DOX complexes in cancer cells under slightly acidic condition was investigated via flow cytometric analysis and fluorescent microscopic study in vitro. After ^{131}I labeling, the radiochemical yield, radiostability in vitro, biodistribution in vivo, SPECT imaging and chemo/radiotherapeutic efficacy of APAS-^{131}I-PNPs/DOX complexes towards cancer cells

and the xenografted tumor model in vivo were systematically assessed. As far as our information goes, this is the first example associated with pH-responsive charge conversional PNPs with ^{131}I labeling on the periphery and complex anticancer drug DOX for enhanced SPECT imaging and chemo/radioactive combination therapy of tumors.

Materials and Methods

Synthesis of APAS-^{131}I-PNPs/DOX Complexes

According to the previous studies, the pH-responsive charge conversional molecule APAS was synthesized and utilized directly.[32,36,48] In the synthesis of APAS-^{131}I-PNPs/DOX complexes, the multifunctional PEI was first prepared using the similar method with our previous researches.[32,43,44,49,50] To be more specific, PEI was successively reacted with mPEG-NHS (15 molar equivalents) and MAL-PEG-SVA (15 molar equivalents) through 3 days continuous stirring to get PEI.NH_2-(mPEG) and PEI.NH_2-(PEG-MAL)-(mPEG) respectively. Then, the obtained PEI.NH_2-(PEG-MAL)-(mPEG) was conjugated with the synthesized APAS (12 molar equivalents) via 24 h reaction between sulfydryl of APAS and MAL moiety of PEI.NH_2-(PEG-MAL)-(mPEG) to form PEI.NH_2-(PEG-APAS)-(mPEG). Later, HPAO (10 molar equivalents) was modified onto the surface of PEI.NH_2-(PEG-APAS)-(mPEG) through the 24 h reaction between N-succinimidyl ester of HPAO and terminal amine of multifunctional PEI. The generated multifunctional PEI.NH_2-HPAO-(PEG-APAS)-(mPEG) was then subjected to the acetylation of terminal amines, which lead to formation of PEI.NHAc-HPAO-(PEG-APAS)-(mPEG). Finally, the obtained reaction mixture was purified using standard procedure of dialysis and lyophilization to produce the powdery product of PEI.NHAc-HPAO-(PEG-APAS)-(mPEG) (for short, APAS-PNPs) refer to our previous researches.[51–54] As a contrast, the non-APAS linked PEI.NHAc-HPAO-(PEG-MAL)-(mPEG) (for short, PNPs) was synthesized and purified using the similar method under identical experimental conditions.

The obtained APAS-PNPs and PNPs were further utilized as nanoplatform to complex with DOX respectively referring to the previous studies.[49,50,53] DOX·HCl (30 molar equivalents) was first dissolved into methanol (500 μL) and neutralized by adding triethylamine (10 μL) to form the pure DOX. Later, the obtained DOX solution was mixed with the generated APAS-PNPs or PNPs aqueous solution and stirred vigorously for 24 h, which lead to the evaporation of methanol. The acquired APAS-PNPs/DOX complexes or PNPs/DOX complexes aqueous solution were subjected to centrifugation to collect the non-complexing free DOX precipitate. Finally, the supernatant of APAS-PNPs/DOX complexes or PNPs/DOX complexes was lyophilized to get the powdery multifunctional PEI/DOX complexes.

According to the facile method of ^{131}I labeling in our previous researches.[43,44,52] The radioactive ^{131}I can be efficiently labeled onto the terminal of PEI via chelate HPAO. To be more specific, the raw Na^{131}I solution (20 mCi, 100 μL) was added into an iodogen-coated glass tube (100 μg). Followed by adding the PBS solution (200 μL, pH 7.4) of APAS-PNPs/DOX complexes (200 μg) or PNPs/DOX complexes (200 μg) into the glass tube and swaying gently for 3 min respectively, the radioactive APAS-^{131}I-PNPs/DOX complexes and ^{131}I-PNPs/DOX complexes were prepared and purified using PD-10 desalting columns.

In vitro Drug Release Kinetics Study

The DOX release kinetics of the generated APAS-PNPs/DOX complexes was evaluated under three different pH conditions (pH 5.0, 6.0, and 7.4). Briefly, triplicate APAS-PNPs/DOX complexes (4 mg) were respectively dispersed in the 1 mL phosphate-citric acid buffer with different pHs (pH 5.0, 6.0, or 7.4), transferred into dialysis bags with an MWCO of 14,000, hermetically tied with string, and put into phosphate-citric acid buffer medium (9 mL) with the corresponding pHs (5.0, 6.0 or 7.4), respectively. The drug release system was put in a vapor-bathing constant temperature vibrator at 37 °C. At different specified time points, the buffer medium (1 mL) was collected and replenished with the corresponding buffer medium with the same volume. The collected buffer medium was detected by a Lambda 25 ultraviolet-visible spectrophotometer (Perkin Elmer, Waltham, MA) to analyze the concentration of released DOX. Meanwhile, the release of free DOX·HCl was carried out using the same method under the pH 7.4 condition.

Cytotoxicity Evaluation

To determine the anticancer efficacy of APAS-PNPs/DOX complexes and APAS-^{131}I-PNPs/DOX complexes towards C6 cells under pH 7.4 or pH 6.0 conditions via simulating the microenvironment of normal tissue or tumor in vitro, Cell Counting Kit-8 (CCK-8) assay was utilized. C6 cells (1.2×10^4 cells/well) were first seeded into a 96-well tissue culture plate and incubated

overnight. Later, the medium in each well was exchanged with fresh DMEM containing free DOX, PNPs/DOX complexes, APAS-PNPs/DOX complexes, ^{131}I-PNPs/DOX complexes, or APAS-^{131}I-PNPs/DOX complexes at different DOX concentrations with different pHs (pH 6.0 and 7.4), respectively. The medium with different pHs were adjusted by phosphate buffer, respectively. Followed by 48 h incubation, CCK-8 assay was performed referring to the previous study.[55] As control, the cytotoxicity of PNPs and APAS-PNPs with the same PEI concentrations of ^{131}I-PNPs/DOX complexes and APAS-^{131}I-PNPs/DOX complexes under pH 7.4 or pH 6.0 condition was also investigated using the similar procedure.

SPECT Imaging of a Xenografted Tumor Model in vivo

All animal experiments were carried out after getting the permission of the ethical committee of Shanghai General Hospital and followed the guidelines of the National Ministry of Health. Four- to six-week old BALB/c nude mice (male, 20–25 g) were purchased from Shanghai Slac Laboratory Animal Center (Shanghai, China) and constructed tumor model by injecting C6 cells with a cell density of 5×10^6 per mouse at their right flank on the basis of the protocols published in our previous researches.[27,43,44,52] Until the xenografted tumor reach a volume of 0.7–1.2 cm^3, the SPECT imaging experiments can be performed.

The mice were first randomly divided into experimental and control groups, and each group contain five mice. Before SPECT imaging, the acquired tumor-bearing mice were fed with water containing KI (1%) to saturate the thyroid uptake of ^{131}I-labeled materials for 3 days to avoid thyroid imaging. Then, the mice were anesthetized by intraperitoneal injection of pentobarbital sodium with a dosage of 40 mg/kg. After that, the PBS solution of APAS-^{131}I-PNPs/DOX complexes ([^{131}I] = 800 μCi, 100 μL) and ^{131}I-PNPs/DOX complexes ([^{131}I] = 800 μCi, 100 μL) were respectively injected into the mice of experimental group and control group intravenously at the same time. At various specific time points (0.5 h, 1 h, 2 h, 4 h, 6 h, 8 h, and 12 h) post-injection, the SPECT images of tumor bearing mice were captured and the corresponding relative SPECT signals were gained from an Infinia SPECT scanner equipped with Xeleris Work Station and a High-Energy General-Purpose detector (GE Inc., Fairfield, CT). At 6 h post-injection, a mouse from each group was randomly selected and sacrificed to harvest major organs and tumors. Later, the relative SPECT signals of these organs and tumors with different treatments were recorded for the biodistribution analysis.

In vivo Antitumor Efficacy

Based on the chemotherapeutic efficacy of free DOX and radiotherapeutic efficacy of ^{131}I, the antitumor efficiency of APAS-^{131}I-PNPs/DOX complexes in vivo was further investigated. The mice were first split into seven groups and each group contain five mice. Each group mice were injected with saline, Na^{131}I ([^{131}I] = 400 μCi), DOX ([DOX] = 1 mg/mL), ^{131}I-PNPs ([^{131}I] = 400 μCi), APAS-^{131}I-PNPs ([^{131}I] = 400 μCi), ^{131}I-PNPs/DOX complexes ([^{131}I] = 400 μCi, [DOX] = 1 mg/mL), or APAS-^{131}I-PNPs/DOX complexes ([^{131}I] = 400 μCi, [DOX] = 1 mg/mL) intravenously at the volume of 100 μL every third day. The whole treatment lasted for 21 days. The antitumor performance was finally evaluated by analyzing the absolute tumor volume, relative tumor volume, body weight, and survival rate of the mice with various treatments following the method published in our previous reports.[27,43,52] In detail, the tumor length and width were measured by a caliper and the absolute tumor volume was calculated according to the equation (tumor length × (tumor width)^2/2). The relative tumor volume (denoted as V/V_0, where V_0 and V are the absolute tumor volumes before the treatment was initiated (ie, day 0) and treated at designated time points, respectively) and body weight of every mouse were recorded at designated time points. The survival rate of the mice in each group was calculated according to the equation of $N_1/N \times 100\%$, where N_1 and N are the number of surviving mice and the number of total mice in each group, respectively. See full experimental details in Supporting Information.

Results and Discussion

Synthesis and Characterization of APAS-^{131}I-PNPs/DOX Complexes

As demonstrated in the synthesis scheme of APAS-^{131}I-PNPs/DOX complexes (Scheme 1), PEI was utilized as the typical nanovehicle to conjugate different moieties (mPEG-NHS, MAL-PEG-SVA, APAS, and HPAO) to achieve multi-functionalization. Followed by loading DOX and radionuclide ^{131}I onto the multifunctional

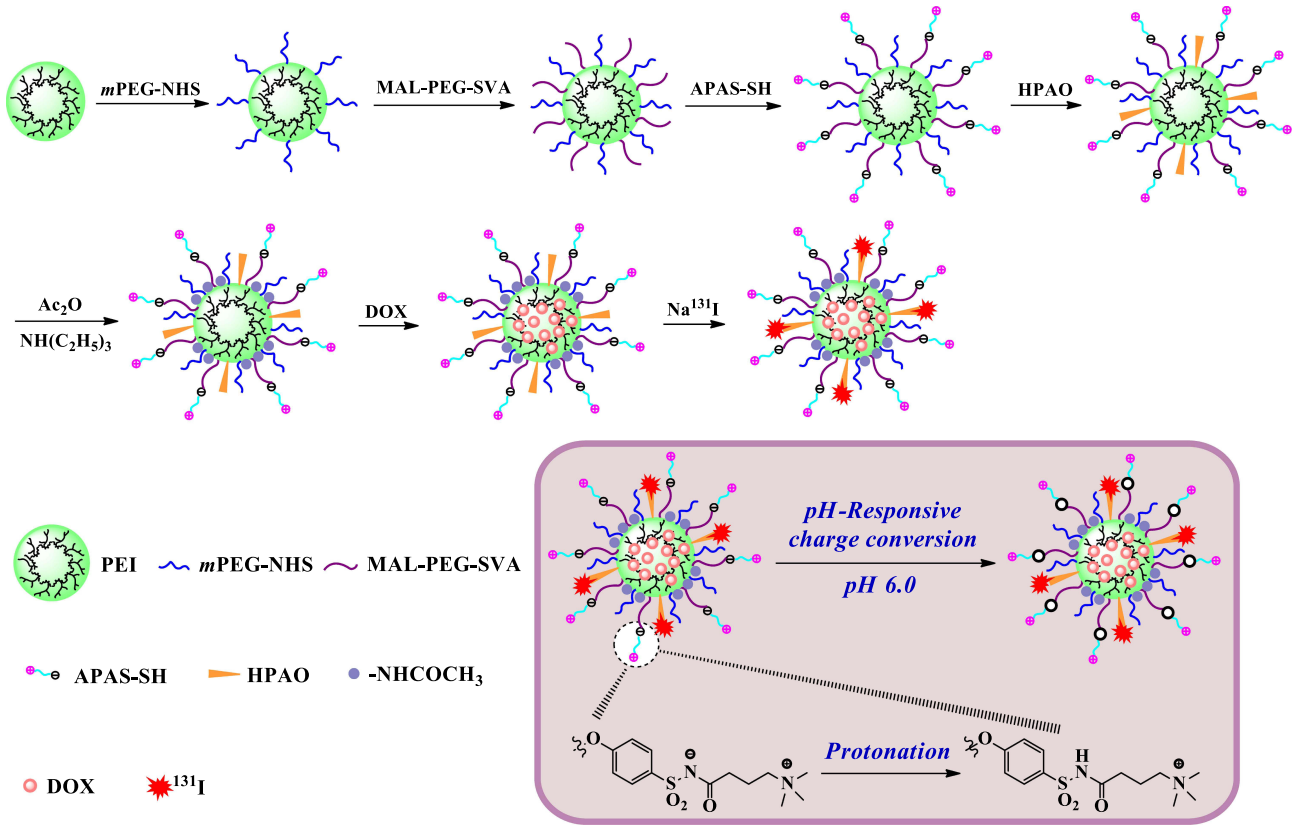

Scheme 1 Schematic representation of the synthesis of APAS-^{131}I-PNPs/DOX complexes.

PEI nanoplatform, the theranostic nanosystem was generated. Based on the experience of previous studies,[53,56,57] partial PEGylation could effectively improve the drug loading efficiency of drug/carrier complex system. Furthermore, according to the APAS-mediated pH-controlled cellular uptake, the novel theranostic nanosystem was expected to achieve enhanced SPECT imaging and chemo/radioactive combination therapy of tumors.

The multifunctional nanoplatform with various conjugations was first characterized and analyzed using ^{1}H NMR spectroscopy and UV-vis spectrometry. The sequentially acquired products, which included PEI.NH_2-(mPEG), PEI.NH_2-(PEG-MAL)-(mPEG), PEI.NH_2-(PEG-APAS)-(mPEG), and PEI.NH_2-HPAO-(PEG-APAS)-(mPEG) were analyzed qualitatively and quantitatively via their ^{1}H NMR spectra (Figure S1). Through verifying and integrating the characteristic peaks of every functional moieties, it can be determined that 12.8 mPEG moieties, 13.5 MAL-PEG-SVA moieties, 6.5 APAS moieties, and 7.3 HPAO moieties were linked to the PEI carrier referring to the calculation method in our previous studies.[27,32,52] The generated multifunctional nanoplatform PEI.NH_2-HPAO-(PEG-APAS)-(mPEG) was then utilized to complex anticancer drug DOX and confirmed by UV-vis spectrometry (Figure S2). Before DOX complexing, the nanoplatform PEI.NH_2-(PEG-APAS)-(mPEG) and PEI.NH_2-HPAO-(PEG-APAS)-(mPEG) do not display the distinct absorption peak, illustrating the functional molecules APAS and HPAO do not own the UV-vis absorption from 400 to 800 nm. After complexing DOX into the APAS-PNPs, the generated APAS-PNPs/DOX complexes demonstrate the typical DOX absorption at 505 nm, suggesting the successful complexation of DOX. In comparison with the absorption peak of free DOX (490 nm), the characteristic peak of APAS-PNPs/DOX complexes is slightly red-shifted due to the weak intermolecular interaction of DOX resulted in the reduced electronic transition after introducing DOX into the multifunctional PEI nanosystem. Through a series of purification processes, the yield of APAS-PNPs/DOX complexes is 68.4%. The DOX loading efficiency of APAS-PNPs/DOX complexes was analyzed with UV-vis spectroscopy based on a standard DOX absorbance/concentration calibration curve, the method is similar to our previous study.[53] It can be calculated that approximately 12.4 DOX molecules complexed with each multifunctional PEI in APAS-PNPs/DOX complexes and the DOX percentage

was reached 8.39%. The similar results can be found in the non-APAS linked PNPs/DOX complexes, there were 12.0 DOX molecules complexed with each multifunctional PEI and the DOX percentage was determined to be 8.75% (Table S1). Atomic force microscopy (AFM) was then utilized to record the morphology and size of APAS-PNPs/DOX complexes. Clearly, the APAS-PNPs/DOX complexes reflect an ellipsoidal structure with the height of 35.6 ± 7.2 nm (Figure 1A and B).

After effectively labeling ^{131}I onto the surface of PEI via HPAO using Iodogen method, the radiochemical yield of ^{131}I-PNPs/DOX complexes and APAS-^{131}I-PNPs/DOX complexes are reached 99.1% ± 0.71% and 99.5% ± 0.21% respectively, which can be used directly without further purification.

pH-Responsive Charge Conversional Function of APAS-PNPs/DOX Complexes

Based on the charge switchable property of APAS under different pH conditions, charge conversional function of APAS-PNPs/DOX complexes should be determined via zeta potential analysis. As Figure 1C revealed the zeta potential of APAS-PNPs/DOX complexes changed from neutral to positive with the decrease in pH value. To be more specific, the APAS-PNPs/DOX complexes is close to neutral under the physiological condition of normal tissues

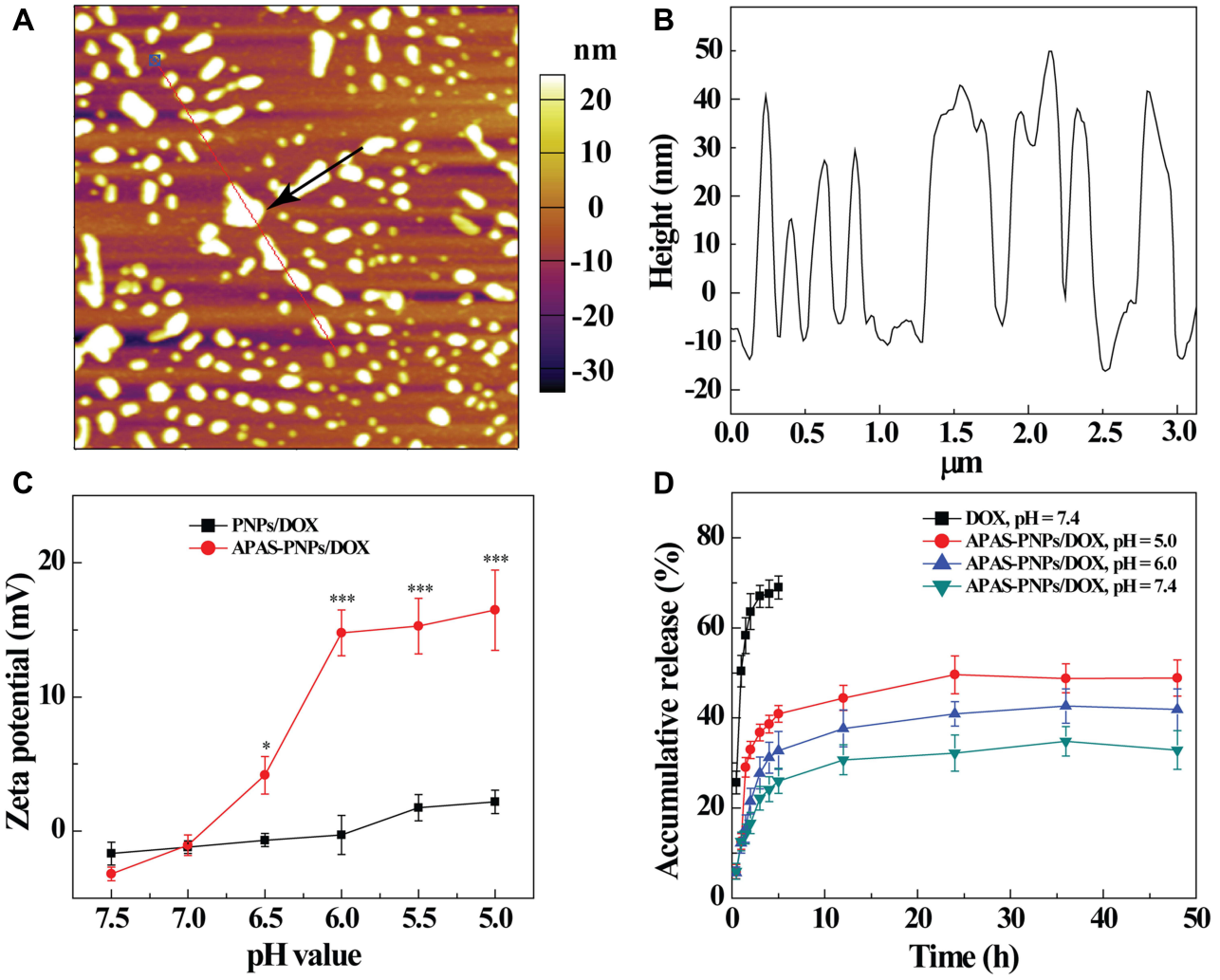

Figure 1 AFM image (**A**) and corresponding height profiles (**B**) of APAS-PNPs/DOX complexes deposited onto silicon wafers. (**C**) Zeta potential plotted against pH values for PNPs/DOX complexes and APAS-PNPs/DOX complexes. Zeta potentials were determined in phosphate buffer at different pH values. All experiments were performed in triplicate, and error bars represent standard error of the mean. (**D**) Cumulative release of DOX from APAS-PNPs/DOX complexes in phosphate-citric acid buffer with different pHs at 37 °C. Cumulative release of free DOX in PBS buffer (pH = 7.4) was performed as control. All experiments were performed in triplicate, and error bars represent standard error of the mean. (*p < 0.05, ***p < 0.001).

(pH 7.0–7.5), and sharply turn to be positive with the increase of acidity (pH 5.0–6.5). When the pH reaches 5.0, the surface zeta potential of APAS-PNPs/DOX complexes is increased up to 16.5 ± 3.00 mV. As control, the zeta potential of non-APAS linked PNPs/DOX complexes ranged from −1.5 mV to 2.2 mV, which always keep the neutral charge with the change of pH value (pH 5.0–7.5). With the APAS coating, the APAS-PNPs/DOX complexes enable surface charge switchable (from neutral to positive) with the decrease of pH (from 7.5 to 5.0) according to the structure characteristics of APAS, which contain negatively charged sulfamine group and positively charged quaternary ammonium group to ensure it keeps neutral at neutral pH environment and turns to be positive at the slightly acidic environment due to protonation onto sulfamine group (Scheme 1). The results fully illustrate APAS-PNPs/DOX complexes own the pH-responsive charge conversional ability due to the APAS surface coating, which provides the possibility for high cellular uptake of APAS-PNPs/DOX complexes in cancer cells via electrostatic binding.

Meanwhile, the hydrodynamic sizes of PNPs/DOX complexes and APAS-PNPs/DOX complexes were determined and analyzed under different pH conditions (Table S2). To be more specific, pH 7.4 and pH 6.0 we selected here to provide the physiological condition of normal tissue and tumor, respectively. It is easy to find that the hydrodynamic size of PNPs/DOX complexes is about 203 nm under various pH conditions, which does not seem to greatly change with the change of acidity (from pH 7.4 to pH 6.0). However, the hydrodynamic size of APAS-PNPs/DOX complexes changes sharply (from 208.21 ± 9.54 nm to 241.16 ± 13.57 nm) with the change of acidity (from pH 7.4 to pH 6.0) due to the protonated APAS to achieve charge conversion, which enlarge the interparticle distance via electrostatic interaction. The hydrodynamic size distribution graphs of PNPs/DOX complexes and APAS-PNPs/DOX complexes under pH 7.4 condition also demonstrate the relatively narrow size distribution (Figure S3). It is easy to find that the hydrodynamic size of APAS-PNPs/DOX complexes is much larger than the size measured by AFM, which attribute to the fact that AFM measure the height of the generated APAS-PNPs/DOX complexes associated with a single nanoparticle. While the hydrodynamic size of APAS-PNPs/DOX complexes obtained from the dynamic light scattering (DLS) tests reflect the size of the clustered APAS-PNPs/DOX complexes, which contain many single particle in aqueous solution. Therefore, the hydrodynamic size of APAS-PNPs/DOX complexes is obviously different with their size measured by AFM, in agreement with the previous report.[49]

In vitro Drug Release Kinetics

In order to exert the chemotherapeutic efficacy of APAS-PNPs/DOX complexes, the release kinetics of free DOX from APAS-PNPs/DOX complexes should be evaluated

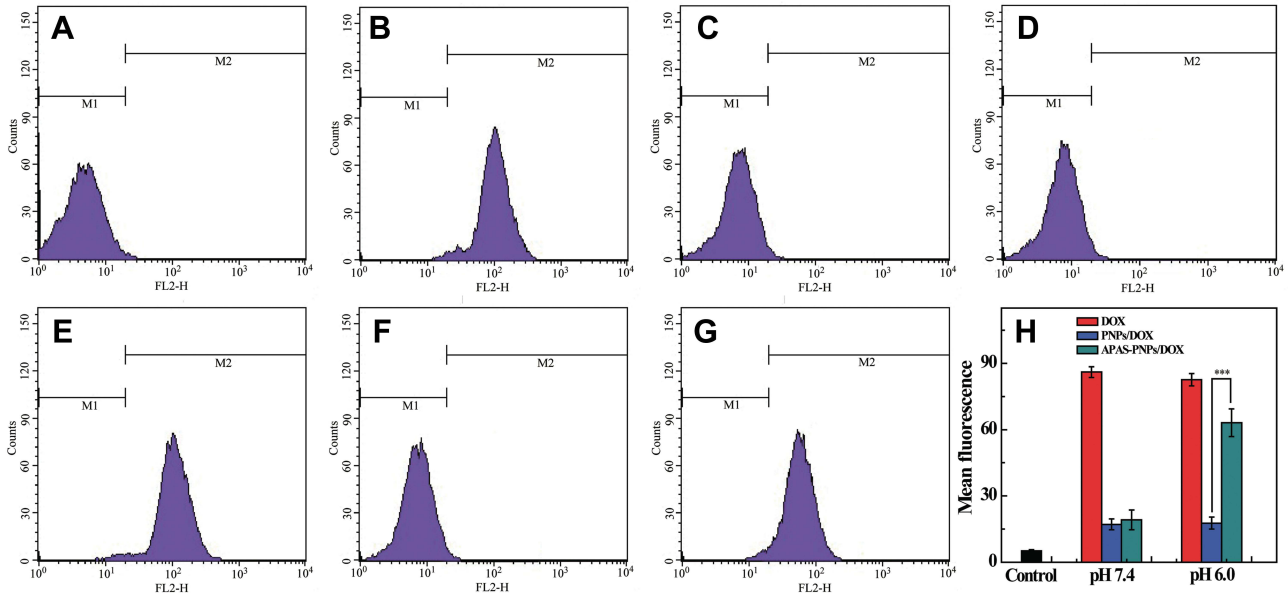

Figure 2 Flow cytometric analysis of C6 cells treated with PBS (**A**), DOX (**B**), PNPs/DOX complexes (**C**), APAS-PNPs/DOX complexes (**D**) at pH 7.4 condition for 3 h. And C6 cells treated with DOX (**E**), PNPs/DOX complexes (**F**), APAS-PNPs/DOX complexes (**G**) at pH 6.0 condition for 3 h, respectively. The DOX concentration for all materials was set at 5 μM. (**H**) shows the comparison of the fluorescence intensity of different materials treated C6 cells at different pH conditions. (***p < 0.001).

in vitro. The APAS-PNPs/DOX complexes demonstrated sustainable release of DOX following a pH-dependent manner (Figure 1D). In contrast, free DOX released rapidly and attained maximum accumulative release (70.0%) within 5 h at pH 7.4 condition, which is identical with the previous reports.[26,53] Here we exposed APAS-PNPs/DOX complexes to phosphate-citric acid buffer with three different pH conditions (pH 5.0, 6.0 and 7.4). With the increase in microenvironment acidity, the DOX release rate increases obviously. After 48 h, 48.9%, 41.9% and 32.9% of DOX is cumulatively released from the APAS-PNPs/DOX complexes at pH 5.0, 6.0 and 7.4, respectively. The acidic microenvironment induced the faster release rates of DOX is likely due to the acidic condition enable the DOX protonated, which may repel the positively charged DOX from the protonated PEI backbone. Moreover, the protonated DOX is quite hydrophilic, which lead to the pH-dependent release behavior of APAS-PNPs/DOX complexes. The result is similar to the drug release kinetics of the PEI-based drug delivery nanosystems in the previous studies.[49,50]

pH-Controlled Cellular Uptake

Based on the confirmed pH-responsive charge conversional function of APAS-PNPs/DOX complexes we described above, the corresponding cellular uptake efficacy should be deeply studied under various pH conditions. Owing to the fluorescence of DOX, the cellular uptake efficiency of APAS-PNPs/DOX complexes can be assessed via flow cytometry (Figure 2) and fluorescent microscopy (Figure 3). In order to provide the physiological condition of normal tissue and tumor, we selected pH 7.4 and pH 6.0 condition for cells incubation, respectively.

After 3 h incubation, the C6 cells subjected to APAS-PNPs/DOX complexes under pH 6.0 condition reveal distinctly higher mean fluorescence intensity than that of cells treated with PNPs/DOX complexes or APAS-PNPs/DOX complexes under pH 7.4 condition and PNPs/DOX complexes under pH 6.0 condition (Figure 2C and D, 2F–H). The cells display relatively low fluorescence intensity after treatment with PNPs/DOX complexes or APAS-PNPs /DOX complexes under pH 7.4 condition or PNPs/DOX complexes under pH 6.0 condition, but show slightly higher fluorescence intensity than PBS incubated cells (Figure 2A). The results indicate APAS-PNPs/DOX complexes could achieve enhanced cellular uptake under slightly acidic environment due to the APAS-mediated charge conversion, which is in agreement with the previous study.[32] It is interesting to note that cells treated with APAS-PNPs/DOX complexes under pH 6.0 condition present lower fluorescence intensity than that of cells treated with free DOX under pH 7.4 condition or pH 6.0 condition, revealing the less cellular uptake of APAS-PNPs/DOX complexes than free DOX (Figure 2B, E and H).

The same results can be confirmed by fluorescent microscopic imaging (Figure 3). The DOX loading enable us to visualize the cellular uptake of the particles. PBS incubated cells do not present any fluorescence signals, while free DOX-treated cells under pH 7.4 condition or pH 6.0 condition demonstrate extremely distinct red fluorescence both in cytoplasma and cell nuclei based on the size advantage of small molecule. APAS-PNPs/DOX complexes incubated cells display significant red fluorescence under pH 6.0 condition, which is attributed to the APAS induced enhanced cellular uptake under slightly acidic environment. In contrast, the cells incubated with PNPs/DOX complexes or APAS-PNPs /DOX complexes under pH 7.4 condition and PNPs/DOX complexes under pH 6.0 condition exhibit extremely weak fluorescence, which is ascribed to the non-specific phagocytosis and diffusion mechanisms through cell walls. These results verify the flow cytometric analysis, validating the APAS-mediated cellular uptake of APAS-PNPs/DOX complexes, which can be controlled by pH.

Stability Evaluation in vitro

Before ^{131}I labeling, the colloidal stability of APAS-PNPs /DOX complexes and PNPs/DOX complexes were evaluated by observing the solution changes after 5 days storage. The generated powder of APAS-PNPs/DOX complexes and PNPs/DOX complexes can be easily dissolved into water and cell culture medium without precipitation occurred, which illuminates the formed DOX complexes are quite stable in different solvents (Figure S4).

After ^{131}I labeling, the traditional instant thin-layer chromatography (ITLC) was utilized to assess the radiostability of ^{131}I-PNPs/DOX complexes and APAS-^{131}I-PNPs/DOX complexes through measuring the radiochemical purities of ^{131}I-PNPs/DOX complexes and APAS-^{131}I-PNPs/DOX complexes, which were exposed to different solvents (PBS and FBS solution) for different time periods. The result indicates the radiochemical purities of ^{131}I-PNPs/DOX complexes and APAS-^{131}I-PNPs/

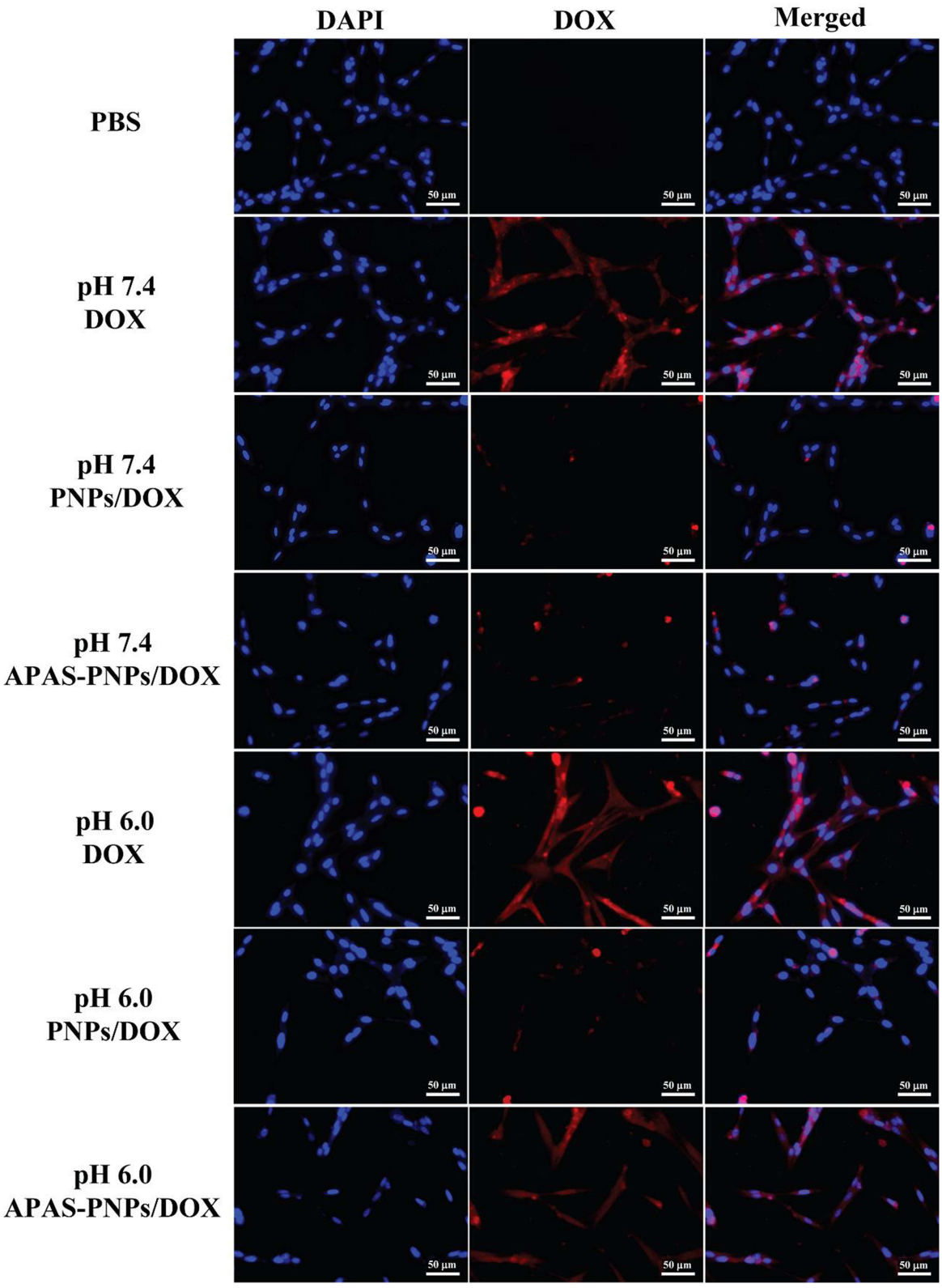

Figure 3 Fluorescent microscopy images of C6 cells treated with PBS, DOX, PNPs/DOX complexes and APAS-PNPs/DOX complexes under various pH conditions for 3 h, respectively. The DOX concentration for all materials was determined to be 5 μM.

DOX complexes are approach to 99% after 1 h, and they maintain at least 95% after 16 h in PBS at room temperature and FBS at 37 °C, which reflects the satisfactory radiostability in vitro (Figure S5).

SPECT Imaging of Cancer Cells

According to the specific properties of APAS and ^{131}I, which could enable enhanced cellular uptake under slightly acidic environment and emit γ-ray for SPECT imaging, respectively, the SPECT imaging efficiency of APAS-^{131}I-PNPs/DOX complexes towards cancer cells should be studied under various pH conditions (pH 6.0 and 7.4). The pH 7.4 and 6.0 conditions are corresponding to the physiological conditions of normal tissue and tumor, respectively. From the SPECT images of C6 cells (Figure 4A), the SPECT signals of cancer cells are increased in a radionuclide dose-dependent manner after treatment with ^{131}I-PNPs/DOX complexes or APAS-^{131}I-PNPs/DOX complexes under different pH conditions. And the cells with APAS-^{131}I-PNPs/DOX complexes treatment display a stronger SPECT signal than those with ^{131}I-PNPs/DOX complexes treatment at the same ^{131}I concentration under pH 6.0 condition. Meanwhile, both the cells treated with ^{131}I-PNPs/DOX complexes and APAS-^{131}I-PNPs/DOX complexes under pH 7.4 condition own the relatively lower signals than those treated with APAS-^{131}I-PNPs/DOX complexes under pH 6.0 condition at the same ^{131}I concentration. The results of quantitative analysis verify the cells with APAS-^{131}I-PNPs/DOX complexes treatment under pH 6.0 condition at various ^{131}I concentrations (100 μCi/mL, 200 μCi/mL, and 400 μCi/mL) have distinct higher SPECT signal intensities than those with ^{131}I-PNPs/DOX complexes and APAS-^{131}I-PNPs/DOX complexes treatments under pH 7.4 condition and those with ^{131}I-PNPs/DOX complexes treatment under pH 6.0 condition at the same ^{131}I concentration ($p < 0.001$, Figure 4B). This acquired result suggests APAS-^{131}I-PNPs/DOX complexes could afford enhanced SPECT imaging of C6 cells due to APAS-mediated enhanced cellular uptake under slightly acidic environment.

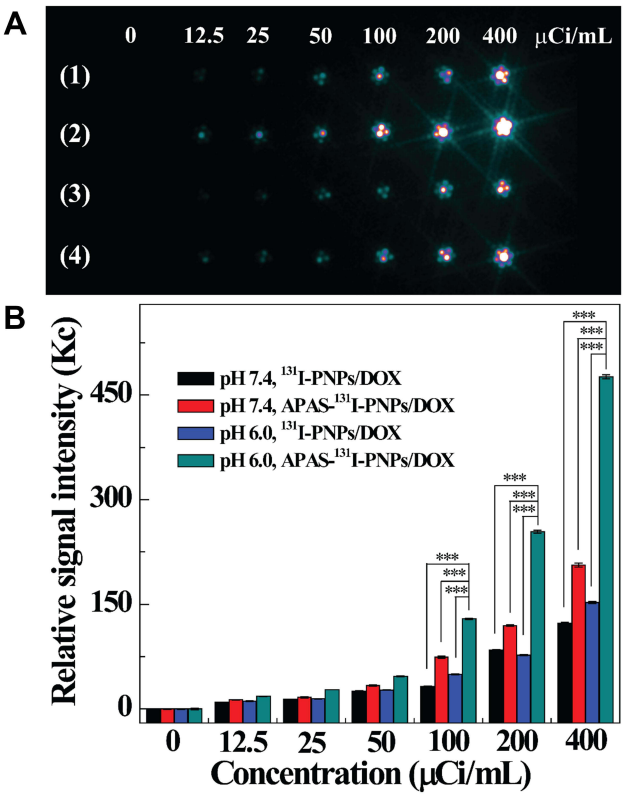

Figure 4 SPECT images (**A**) and the related SPECT signals (**B**) of the C6 cells with treatment of ^{131}I-PNPs/DOX complexes (1) and APAS-^{131}I-PNPs/DOX complexes (2) under pH 6.0 condition at different ^{131}I concentrations (μCi/mL) for 3 h. And C6 cells with treatment of ^{131}I-PNPs/DOX complexes (3) and APAS-^{131}I-PNPs/DOX complexes (4) under pH 7.4 condition at different ^{131}I concentrations (μCi/mL) for 3 h, respectively. (***$p < 0.001$).

Cytotoxicity Evaluation

After loading DOX and ^{131}I into the unique PEI-based theranostic nanosystem, the cytotoxicity of APAS-PNPs /DOX complexes, APAS-^{131}I-PNPs/DOX complexes and APAS-PNPs towards C6 cells under various pH conditions was next explored using CCK-8 assay. As demonstrated in Figure 5A, the growth of C6 cells is inhibited in a DOX concentration-dependent manner after treatment with free DOX, PNPs/DOX complexes, APAS-PNPs/DOX complexes, ^{131}I-PNPs/DOX complexes, and APAS-^{131}I-PNPs/DOX complexes under different pH conditions (pH 6.0 and 7.4) for 48 h. After introducing ^{131}I to PNPs/DOX complexes or APAS-PNPs/DOX complexes, the generated ^{131}I-PNPs/DOX complexes or APAS-^{131}I-PNPs/DOX complexes demonstrated stronger cytotoxicity than that of PNPs/DOX complexes or APAS-PNPs/DOX complexes under different pH conditions due to the chemo/radioactive combination therapy of DOX and ^{131}I. It is interesting to note that under pH 6.0 condition, APAS-^{131}I-PNPs/DOX complexes demonstrate distinct higher cell inhibition efficiency than that of ^{131}I-PNPs/DOX complexes at the same pH condition ($p < 0.01$) and that of APAS-^{131}I-PNPs/DOX complexes under pH 7.4 condition ($p < 0.01$), as a result of APAS-mediated charge conversion mechanism at slightly acidic environment, which induced enhanced cellular uptake.

Excluding cytotoxic effect of DOX and ^{131}I, PNPs and APAS-PNPs do not display appreciable cytotoxicity under pH 7.4 condition at the highest concentration tested (119.0 μg/mL). And the studied PNPs or APAS-PNPs concentrations are consistent with the PEI concentrations of ^{131}I-PNPs/DOX complexes or APAS-^{131}I-PNPs/DOX complexes in Figure 5A. However, APAS-PNPs own the slightly cytotoxicity under pH 6.0 condition, which induce the cell viabilities below 80% when the concentration grows up to 95.2 μg/mL (Figure 5B). It is likely due to the APAS-mediated charge conversion (from neutral to positive) at slightly acidic environment, which induced certain cytotoxicity. In general, the APAS modification, DOX complexing, and ^{131}I labeling are all contributed to enhancing the anticancer efficiency of APAS-^{131}I-PNPs/DOX complexes in vitro under slightly acidic environment.

SPECT Imaging of a Xenografted Tumor Model in vivo

The feasibility of using APAS-^{131}I-PNPs/DOX complexes for enhanced SPECT imaging of tumor in vivo was further investigated after validating the APAS-mediated improved SPECT imaging of C6 cells via simulating the microenvironment of tumor in vitro. As shown in Figure 6A, there is no appreciable tumor SPECT signal after treatment with either ^{131}I-PNPs/DOX complexes or APAS-^{131}I-PNPs/DOX complexes for 0.5 h, 1 h, and 2 h. At 4 h, 6 h, 8 h, and 12 h post-injection, APAS-^{131}I-PNPs/DOX complexes treated tumor-bearing mice demonstrate much higher tumor SPECT signals than that of ^{131}I-PNPs/DOX complexes treated tumor-bearing mice. Through quantitative analysis of the relative SPECT signal intensities of tumors (Figure 6B), it can be found that the tumor-bearing mice with APAS-^{131}I-PNPs/DOX complexes treatment own the significantly higher SPECT signal intensities of tumor than those of tumor-bearing mice with ^{131}I-PNPs/DOX complexes treatment from 1 h to 12 h post-injection ($p < 0.001$). The relative SPECT signal intensities of tumor with APAS-^{131}I-PNPs/DOX complexes treatment increases from 0.5 h to 4 h, then descends from 6 h to 12 h, which always maintain the relative high SPECT signal intensity. In contrast, the relative SPECT signal intensities of tumor with ^{131}I-PNPs/DOX complexes treatment keep the relative low signal level. The quantitative analysis result is identical with the SPECT images of tumor-bearing mice after various treatments. The significant difference in tumor SPECT signal of mice treated with ^{131}I-PNPs/DOX complexes or APAS-^{131}I-PNPs/DOX complexes was further verified by the SPECT imaging of ex vivo tumor at 6 h post-injection. It is obvious that the tumor with APAS-^{131}I-PNPs/DOX complexes treatment display much higher SPECT signal than that of the tumor with ^{131}I-PNPs/DOX complexes treatment (Figure 6C).

The biodistribution of APAS-^{131}I-PNPs/DOX complexes or ^{131}I-PNPs/DOX complexes at 6 h post-injection was finally studied via SPECT imaging in vivo (Figure

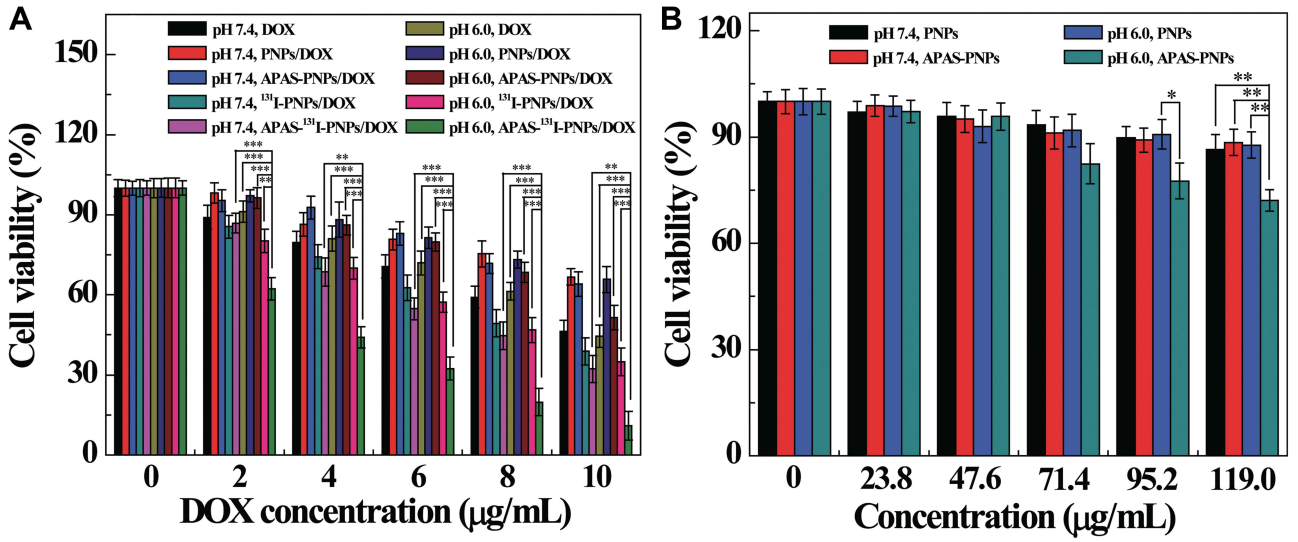

Figure 5 (**A**) CCK-8 assay of C6 cells treated with DOX, PNPs/DOX complexes, APAS-PNPs/DOX complexes, ^{131}I-PNPs/DOX complexes, or APAS-^{131}I-PNPs/DOX complexes at different DOX concentrations under various pH conditions for 48 h, respectively. (**B**) CCK-8 assay of C6 cells treated with PNPs or APAS-PNPs with the same PEI concentrations of ^{131}I-PNPs/DOX complexes or APAS-^{131}I-PNPs/DOX complexes for 48 h, respectively. (*$p < 0.05$, **$p < 0.01$, ***$p < 0.001$).

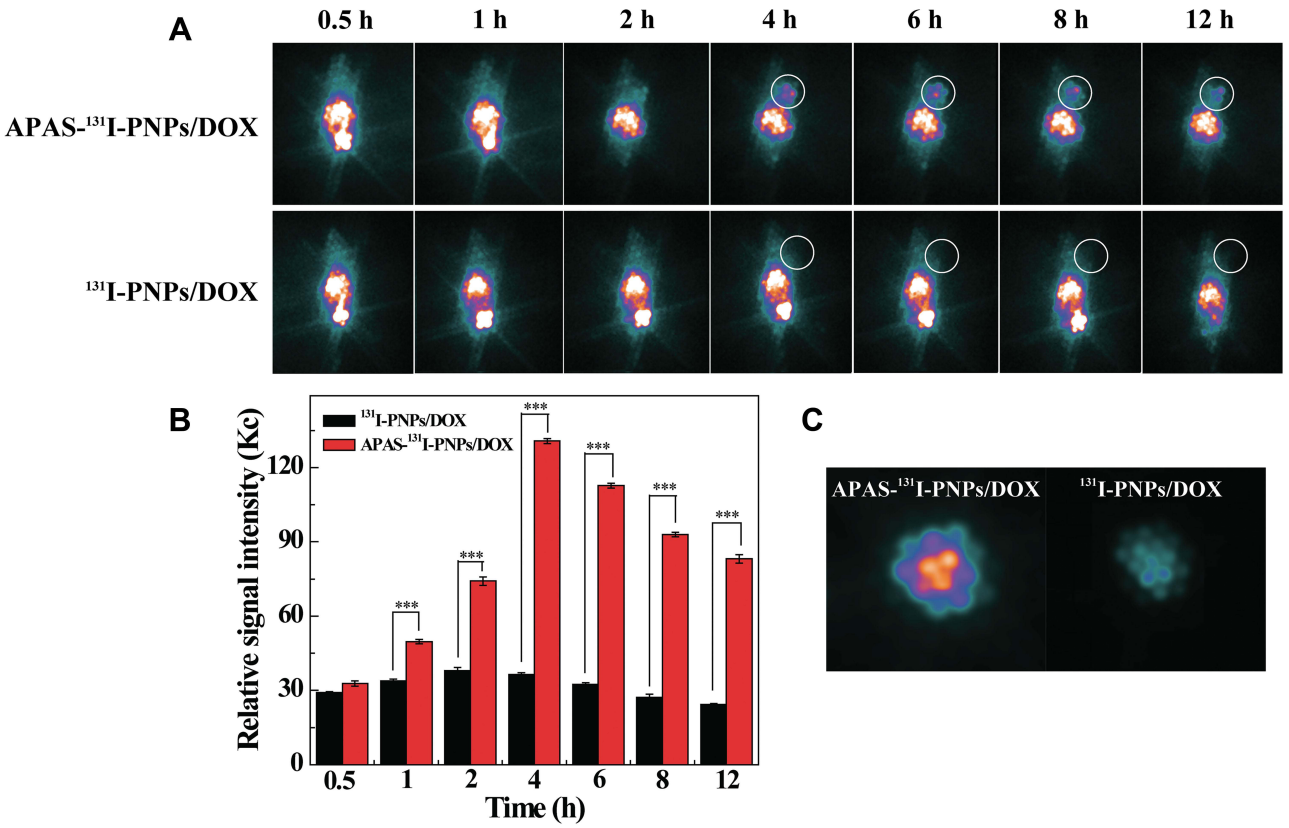

Figure 6 SPECT images of C6 tumor-bearing mice (**A**) and the related SPECT signal intensities of tumors (**B**) at different time points post-injection of APAS-^{131}I-PNPs/DOX complexes and ^{131}I-PNPs/DOX complexes. (**C**) shows the SPECT images of ex vivo tumors at 6 h post-injection. The white circle indicates the tumor site. (***p < 0.001).

S6). Large amount of APAS-^{131}I-PNPs/DOX complexes and ^{131}I-PNPs/DOX complexes are accumulated in liver and intestines, while relatively small amount of APAS-^{131}I-PNPs/DOX complexes and ^{131}I-PNPs/DOX complexes are distributed to heart, lung, stomach, spleen, kidneys, soft tissues, and tumor. Through further analysis, it is easy to find that the tumor accumulation of APAS-^{131}I-PNPs/DOX complexes is distinctly higher than that of ^{131}I-PNPs/DOX complexes ($p < 0.001$), which confirms the specific internalization function mediated by APAS.

In vivo Antitumor Efficacy

The proved anticancer effect in vitro of the generated APAS-^{131}I-PNPs/DOX complexes inspired us to further explore their antitumor efficacy in vivo. As demonstrated in Figure 7A and S7, the tumor-bearing mice with Na^{131}I, DOX, ^{131}I-PNPs, APAS-^{131}I-PNPs, ^{131}I-PNPs/DOX complexes, and APAS-^{131}I-PNPs/DOX complexes treatment all display certain tumor growth inhibition effect after the whole treatment. However, APAS-^{131}I-PNPs/DOX complexes own the best tumor growth inhibition efficiency towards tumor-bearing mice. And the tumor growth rate of tumor-bearing mice with APAS-^{131}I-PNPs/DOX complexes treatment is significantly lower than the mice treated with saline ($p < 0.001$), Na^{131}I ($p < 0.001$), DOX ($p < 0.001$), ^{131}I-PNPs ($p < 0.001$), APAS-^{131}I-PNPs ($p < 0.001$) and ^{131}I-PNPs/DOX complexes ($p < 0.05$) after 21 days' treatment. From the relative tumor volumes we recorded at the 21st day, it can be summarized the tumor growth inhibition follows the order of APAS-^{131}I-PNPs/DOX complexes (5.43 ± 1.65 times) > ^{131}I-PNPs/DOX complexes (9.38 ± 1.58 times) > APAS-^{131}I-PNPs (13.44 ± 2.29 times) > ^{131}I-PNPs (18.48 ± 1.69 times) > Na^{131}I (25.26 ± 2.39 times) > saline (30.58 ± 1.35 times) (Figure 7A). Based on the result that the tumor inhibition efficacy of mice treated with APAS-^{131}I-PNPs/DOX complexes is lower than that of mice with ^{131}I-PNPs/DOX

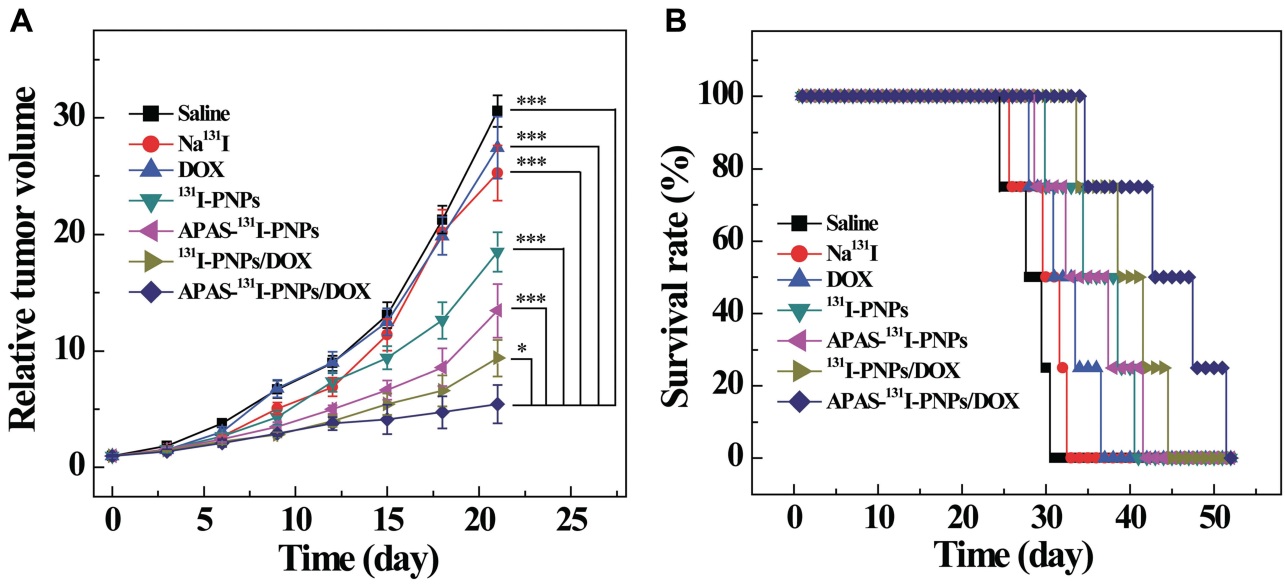

Figure 7 (**A**) Growth of C6 tumors after various treatments. The relative tumor volume was recorded referring to their initial tumor volume in each group. (**B**) Survival rate of C6 tumor-bearing mice after various treatments. (*p < 0.05, ***p < 0.001).

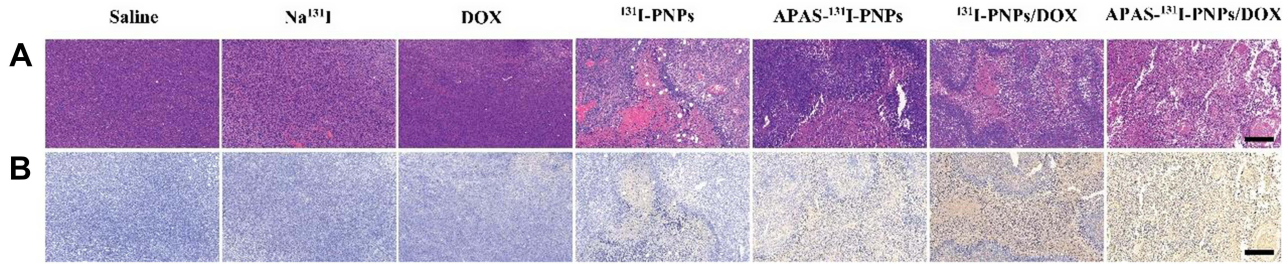

Figure 8 Representative H&E staining (**A**) and TUNEL assay (**B**) of C6 tumors with treatment of various materials, respectively. The scale bar shown in both panels represents 200 μm.

complexes treatment ($p < 0.05$), it reveals the antitumor efficacy is not only associated with the DOX and ^{131}I, but also contributed by the APAS's modification, which enable the improved cellular uptake under the tumor microenvironment and further enhanced the tumor chemo/radio therapeutic efficacy. Combining the function of APAS, DOX, and ^{131}I, APAS-^{131}I-PNPs/DOX complexes could exert their enhanced antitumor efficacy in vivo. Furthermore, the antitumor efficacy was also verified by the survival rates of mice (Figure 7B). The tumor-bearing mice with APAS-^{131}I-PNPs/DOX complexes treatment display the longest survival time (51 days) among tumor-bearing mice with other various treatments. All the tumor-bearing mice treated with ^{131}I-PNPs/DOX complexes, APAS-^{131}I-PNPs, ^{131}I-PNPs, Na^{131}I, DOX, and saline respectively are dead after 45 days. The mice treated with APAS-^{131}I-PNPs/DOX complexes keep a 50% survival rate at 45th day and are all dead after 51 days. The survival rate result clearly manifests APAS-^{131}I-PNPs/DOX complexes could effectively prolong the lifetime of tumor-bearing mice in 21 days treatment, suggesting the improved therapeutic efficacy of APAS-^{131}I-PNPs/DOX complexes indirectly. In addition, there was no significant difference in change of body weight after treatment with saline, DOX, Na^{131}I, ^{131}I-PNPs, APAS-^{131}I-PNPs, ^{131}I-PNPs/DOX complexes, and APAS-^{131}I-PNPs/DOX complexes, respectively (Figure S8). This illustrates the good biocompatibility of APAS-^{131}I-PNPs/DOX complexes, which do not cause distinct toxicity in vivo.

H&E Staining and TUNEL Assay

To further evaluate the improved antitumor efficiency of APAS-^{131}I-PNPs/DOX complexes, hematoxylin and eosin (H&E) staining and terminal deoxynucleotidyl transferase

dUTP nick end labeling (TUNEL) assay were performed (Figure 8). Through treatment of $Na^{131}I$, DOX, ^{131}I-PNPs, APAS-^{131}I-PNPs, ^{131}I-PNPs/DOX complexes, and APAS-^{131}I-PNPs/DOX complexes, respectively, certain degree of necrosis can be found in the H&E stained samples and necrotic area follows the order of $Na^{131}I$ < ^{131}I-PNPs < APAS-^{131}I-PNPs < ^{131}I-PNPs/DOX complexes < APAS-^{131}I-PNPs/DOX complexes (Figure 8A). TUNEL assay reveals the same result with H&E stain, APAS-^{131}I-PNPs/DOX complexes treated tumor-bearing mice own the largest positive staining area of the apoptotic cells in tumor. Other ^{131}I-labeled substances and DOX can also cause certain area of apoptotic cells due to their relative weak anticancer effect in vivo (Figure 8B). The cell apoptosis rate (percentages of TUNEL-positive cells) was further recorded from the TUNEL stained slices (Figure S9). Through statistical analysis, the cell apoptosis rate follows the sequence of APAS-^{131}I-PNPs/DOX complexes (87.25%) > ^{131}I-PNPs/DOX complexes (69.37%) > APAS-^{131}I-PNPs (55.84%) > ^{131}I-PNPs (39.56%) > $Na^{131}I$ (11.13%) > saline (4.50%). And the APAS-^{131}I-PNPs/DOX complexes treated tumor-bearing mice have much higher apoptosis rate of cancer cell than those of other ^{131}I-labeled substances ($p < 0.01$) and DOX ($p < 0.001$). In short, the H&E and TUNEL stain results confirm the enhanced tumor chemo/radiotherapy of APAS-^{131}I-PNPs/DOX complexes based on the APAS-mediated improved cellular uptake under tumor microenvironment.

Finally, the potential toxicity of the ^{131}I-labeled substances and DOX was studied via H&E staining of the major organs (Figure 9). Apparently, there is no distinct organ damage or appreciable abnormality in the major organ slices, revealing the excellent organ compatibility and biosafety of the generated APAS-^{131}I-PNPs/DOX complexes in vivo.

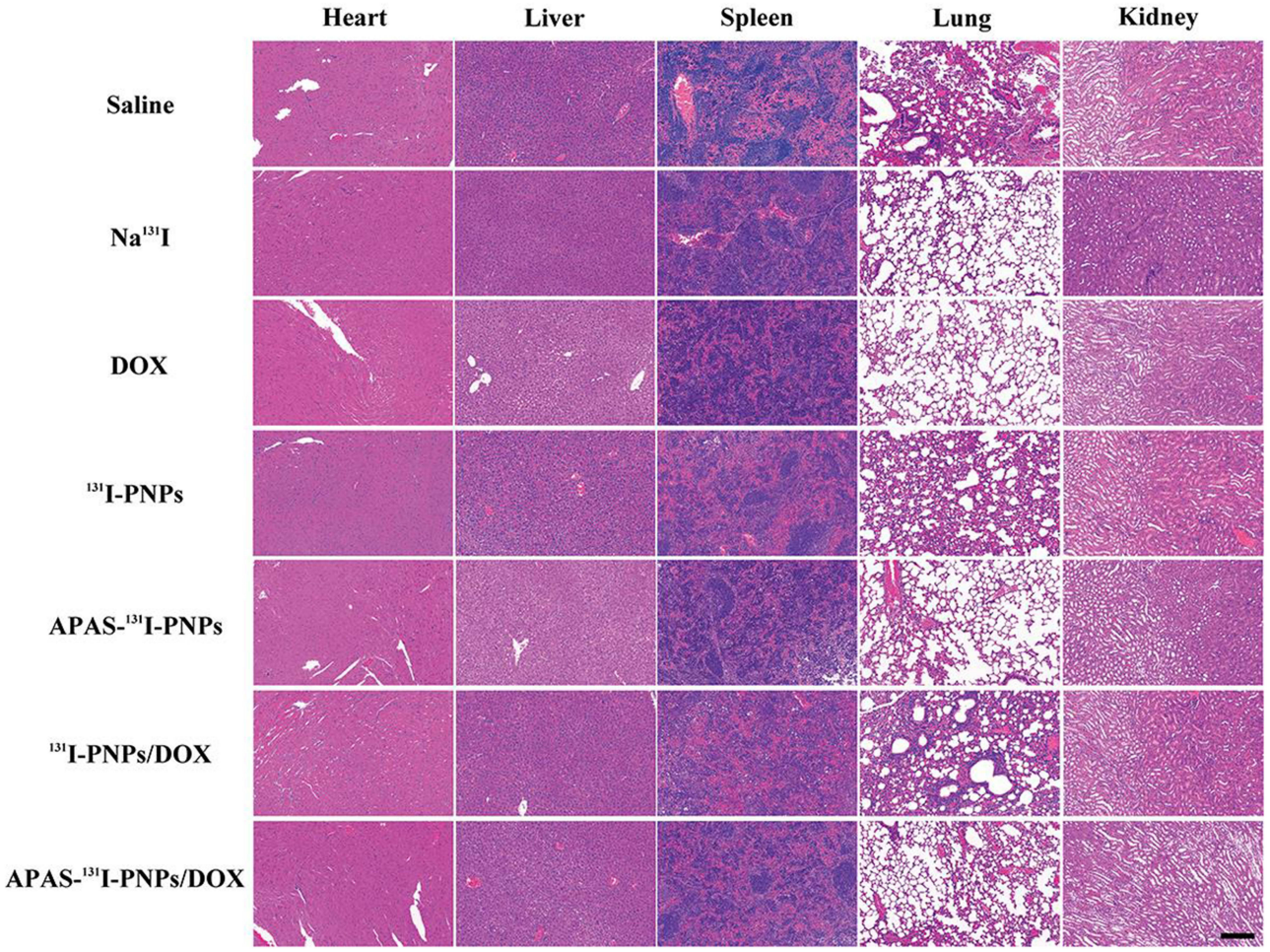

Figure 9 Representative H&E staining of major organs from survived mice with treatment of various materials, respectively. The scale bar (applied for all panels) represents 200 μm.

There is a series of iodine-based nuclides, such as iodine-123 (^{123}I), iodine-125 (^{125}I) and ^{131}I. It seems that ^{123}I has better physical properties than ^{131}I for SPECT imaging according its shorter half-life (13.2 h) and lower photon energy (159 KeV). However, ^{123}I is difficult to produce in domestic and expensive to import from abroad. Considering the low cost and commercial availability, ^{131}I is the preferred radionuclide in this study, which enables simultaneous SPECT imaging and radiotherapy of tumor.

Conclusion

In summary, we built a smart ^{131}I-labeled multifunctional PEI/DOX complexes with pH-controlled cellular uptake function for enhanced SPECT imaging and chemo/radiotherapy of tumors. Via the unique PEI nanotechnology, functional PEG, APAS, and HPAO can be effectively conjugated onto the surface of PEI, followed by complexing DOX and labeling ^{131}I to acquire the novel theranostic nanosystems. The synthesized APAS-PNPs/DOX complexes exhibit favorable water solubility and stability, which could achieve sustainable release of DOX following a pH-dependent manner. Remarkably, with the APAS linking, the APAS-PNPs/DOX complexes enable surface charge switchable (from neutral to positive) with the decrease in pH (from 7.5 to 5.0) according to the structure characteristics of APAS, which contain negatively charged sulfamine group and positively charged quaternary ammonium group to ensure it keeps neutral at neutral pH environment and turns to be positive at the slightly acidic environment due to protonation onto sulfamine group. The constructed theranostic nanosystems own the capacity to achieve pH-responsive charge conversion and further lead to improved cellular uptake in cancer cells under slightly acidic condition, which afford enhanced SPECT imaging and chemo/radioactive combination therapy of cancer cells in vitro and xenografted tumor model in vivo. The developed smart theranostic nanosystem is beneficial for extending a variety of novel nanosystems to improve the tumor theranostic efficiency of different types of cancer.

Acknowledgments

The study is financially supported by the National Natural Science Foundation of China (21807059, 81801727 and 81971647), the Natural Science Foundation of Jiangsu Province (BK20180711), the Natural Science Foundation for Colleges and Universities in Jiangsu Province (17KJB350005), Postgraduate Research & Practice Innovation Program of Jiangsu Province (KYCX20_1122) and the Ningxia Key Research and Development Program (2019BEG03018).

Disclosure

The authors declare no conflicts of interest in this work.

References

1. Feng LL, Gai SL, Dai YL, et al. Controllable generation of free radicals from multifunctional heat-responsive nanoplatform for targeted cancer therapy. *Chem Mater*. 2018;30(2):526–539. doi:10.1021/acs.chemmater.7b04841
2. Sun QQ, Bi HT, Wang Z, et al. Hyaluronic acid-targeted and pH-responsive drug delivery system based on metal-organic frameworks for efficient antitumor therapy. *Biomaterials*. 2019;223:119473. doi:10.1016/j.biomaterials.2019.119473
3. Sun QQ, He F, Bi HT, et al. An intelligent nanoplatform for simultaneously controlled chemo-, photothermal, and photodynamic therapies mediated by a single NIR light. *Chem Eng J*. 2019;362:679–691. doi:10.1016/j.cej.2019.01.095
4. Albuquerque LJC, Sincari V, Jäger A, et al. pH-responsive polymersome-mediated delivery of doxorubicin into tumor sites enhances the therapeutic efficacy and reduces cardiotoxic effects. *J Control Release*. 2021;332:529–538. doi:10.1016/j.jconrel.2021.03.013
5. Cui C, Yu P, Wu M, et al. Reduction-sensitive micelles with sheddable PEG shells self-assembled from a Y-shaped amphiphilic polymer for intracellular doxorubicin release. *Colloids Surf B*. 2015;129:137–145. doi:10.1016/j.colsurfb.2015.03.040
6. Cytryniak A, Nazaruk E, Bilewicz R, et al. Lipidic cubic-phase nanoparticles (cubosomes) loaded with doxorubicin and labeled with Lu-177 as a potential tool for combined chemo and internal radiotherapy for cancers. *Nanomaterials*. 2020;10(11):2272. doi:10.3390/nano10112272
7. Hruby M, Kucka J, Konak C, Vetrik M, Lebeda O, Ulbrich K. Thermoresponsive polymer for local chemoradiotherapy with doxorubicin bound via a newly developed hydrolytically labile bond. *J Control Release*. 2008;132(3):E40–E41. doi:10.1016/j.jconrel.2008.09.026
8. Hruby M, Kucka J, Mackova H, et al. New binary thermoresponsive polymeric system for local chemoradiotherapy. *J Appl Polym Sci*. 2009;111(5):2220–2228. doi:10.1002/app.29237
9. Sedlacek O, Monnery BD, Mattova J, et al. Poly(2-ethyl-2-oxazoline) conjugates with doxorubicin for cancer therapy: in vitro and in vivo evaluation and direct comparison to poly N-(2-hydroxypropyl)methacrylamide analogues. *Biomaterials*. 2017;146:1–12. doi:10.1016/j.biomaterials.2017.09.003
10. Hartshorn CM, Bradbury MS, Lanza GM, et al. Nanotechnology strategies to advance outcomes in clinical cancer care. *ACS Nano*. 2018;12(1):24–43. doi:10.1021/acsnano.7b05108
11. Wang Y, Sun S, Zhang Z, Shi D. Nanomaterials for cancer precision medicine. *Adv Mater*. 2018;30(17):1705660. doi:10.1002/adma.201705660
12. Falagan-Lotsch P, Grzincic EM, Murphy CJ. New advances in nanotechnology-based diagnosis and therapeutics for breast cancer: an assessment of active-targeting inorganic nanoplatforms. *Bioconjug Chem*. 2017;28(1):135–152. doi:10.1021/acs.bioconjchem.6b00591
13. Guo B, Zhao J, Zhang Z, An X, Huang M, Wang S. Intelligent nanoenzyme for T_1-weighted MRI guided theranostic applications. *Chem Eng J*. 2020;391:123609. doi:10.1016/j.cej.2019.123609

14. Xu Y, Zhao J, Zhang Z, et al. Preparation of electrospray ALG/PDA-PVP nanocomposites and their application in cancer therapy. *Soft Matter*. 2020;16(1):132–141. doi:10.1039/C9SM01584A
15. Zheng Y, Wang W, Zhao J, et al. Preparation of injectable temperature-sensitive chitosan-based hydrogel for combined hyperthermia and chemotherapy of colon cancer. *Carbohydr Polym*. 2019;222:115039. doi:10.1016/j.carbpol.2019.115039
16. Liu Y, Xi Y, Zhao J, et al. Preparation of therapeutic-laden konjac hydrogel for tumor combination therapy. *Chem Eng J*. 2019;375:122048. doi:10.1016/j.cej.2019.122048
17. Wu H, Wang W, Zhang Z, et al. Synthesis of a clay-based nanoagent for photonanomedicine. *ACS Appl Mater Interfaces*. 2020;12(1):390–399. doi:10.1021/acsami.9b19930
18. Zhou Y, Jing X, Chen Y. Material chemistry of graphene oxide-based nanocomposites for theranostic nanomedicine. *J Mater Chem B*. 2017;5(32):6451–6470. doi:10.1039/c7tb00680b
19. Chen Y-W, Liu T-Y, Chen P-J, Chang P-H, Chen S-Y. A high-sensitivity and low-power theranostic nanosystem for cell SERS imaging and selectively photothermal therapy using anti-EGFR-conjugated reduced graphene oxide/mesoporous silica/AuNPs nanosheets. *Small*. 2016;12(11):1458–1468. doi:10.1002/smll.201502917
20. Augustine S, Singh J, Srivastava M, Sharma M, Das A, Malhotra BD. Recent advances in carbon based nanosystems for cancer theranostics. *Biomater Sci*. 2017;5(5):901–952. doi:10.1039/c7bm00008a
21. d'Angelo M, Castelli V, Benedetti E, et al. Theranostic nanomedicine for malignant gliomas. Review. *Front Bioeng Biotechnol*. 2019;7(325). doi:10.3389/fbioe.2019.00325
22. Jin Y, Zhang N, Li C, Pu K, Ding C, Zhu Y. Nanosystem composed with MSNs, gadolinium, liposome and cytotoxic peptides for tumor theranostics. *Colloids Surf B*. 2017;151:240–248. doi:10.1016/j.colsurfb.2016.12.024
23. Feng L, Cheng L, Dong Z, et al. Theranostic liposomes with hypoxia-activated prodrug to effectively destruct hypoxic tumors post-photodynamic therapy. *ACS Nano*. 2017;11(1):927–937. doi:10.1021/acsnano.6b07525
24. Li W, Peng J, Yang Q, et al. α-Lipoic acid stabilized DTX/IR780 micelles for photoacoustic/fluorescence imaging guided photothermal therapy/chemotherapy of breast cancer. *Biomater Sci*. 2018;6(5):1201–1216. doi:10.1039/c8bm00096d
25. Li Volsi A, Fiorica C, D'Amico M, et al. Hybrid gold/silica/quantum-dots supramolecular-nanostructures encapsulated in polymeric micelles as potential theranostic tool for targeted cancer therapy. *Eur Polym J*. 2018;105:38–47. doi:10.1016/j.eurpolymj.2018.05.013
26. Zhu J, Wang G, Alves CS, et al. Multifunctional dendrimer-entrapped gold nanoparticles conjugated with doxorubicin for pH-responsive drug delivery and targeted computed tomography imaging. *Langmuir*. 2018;34(41):12428–12435. doi:10.1021/acs.langmuir.8b02901
27. Zhu JY, Zheng LF, Wen SH, et al. Targeted cancer theranostics using alpha-tocopheryl succinate-conjugated multifunctional dendrimer-entrapped gold nanoparticles. *Biomaterials*. 2014;35(26):7635–7646. doi:10.1016/j.biomaterials.2014.05.046
28. Li X, Xing L, Zheng K, et al. Formation of gold nanostar-coated hollow mesoporous silica for tumor multimodality imaging and photothermal therapy. *ACS Appl Mater Interfaces*. 2017;9(7):5817–5827. doi:10.1021/acsami.6b15185
29. Du Y, Jiang Q, Beziere N, et al. DNA-nanostructure-gold-nanorod hybrids for enhanced *in vivo* optoacoustic imaging and photothermal therapy. *Adv Mater*. 2016;28(45):10000–10007. doi:10.1002/adma.201601710
30. Li M, Luo Z, Zhao Y. Self-assembled hybrid nanostructures: versatile multifunctional nanoplatforms for cancer diagnosis and therapy. *Chem Mater*. 2018;30(1):25–53. doi:10.1021/acs.chemmater.7b03924
31. Zhang L, Sheng D, Wang D, et al. Bioinspired multifunctional melanin-based nanoliposome for photoacoustic/magnetic resonance imaging-guided efficient photothermal ablation of cancer. *Theranostics*. 2018;8(6):1591–1606. doi:10.7150/thno.22430
32. Zhu J, Zhao L, Yang J, et al. ^{99m}Tc-Labeled polyethylenimine-entrapped gold nanoparticles with pH-responsive charge conversion property for enhanced dual mode SPECT/CT imaging of cancer cells. *Langmuir*. 2019;35(41):13405–13412. doi:10.1021/acs.langmuir.9b02617
33. Saleem J, Wang L, Chen C. Carbon-based nanomaterials for cancer therapy via targeting tumor microenvironment. *Adv Healthcare Mater*. 2018;7(20):1800525. doi:10.1002/adhm.201800525
34. Li Y, Hong W, Zhang H, et al. Photothermally triggered cytosolic drug delivery of glucose functionalized polydopamine nanoparticles in response to tumor microenvironment for the GLUT1-targeting chemo-phototherapy. *J Control Release*. 2020;317:232–245. doi:10.1016/j.jconrel.2019.11.031
35. Wang J, Wang X, Lu S-Y, et al. Integration of cascade delivery and tumor hypoxia modulating capacities in core-releasable satellite nanovehicles to enhance tumor chemotherapy. *Biomaterials*. 2019;223:119465. doi:10.1016/j.biomaterials.2019.119465
36. Mizuhara T, Saha K, Moyano DF, et al. Acylsulfonamide-functionalized zwitterionic gold nanoparticles for enhanced cellular uptake at tumor pH. *Angew Chem Int Ed*. 2015;54(22):6567–6570. doi:10.1002/anie.201411615
37. Wang S, Huang P, Chen X. Stimuli-responsive programmed specific targeting in nanomedicine. *ACS Nano*. 2016;10(3):2991–2994. doi:10.1021/acsnano.6b00870
38. Zou Y, Li D, Shen M, Shi X. Polyethylenimine-based nanogels for biomedical applications. *Macromol Biosci*. 2019;19(11):1900272. doi:10.1002/mabi.201900272
39. Lan S, Xie W, Wang J, et al. PEGylated polyethylenimine-stabilized polypyrrole nanoparticles loaded with DOX for chemo-photothermal therapy of cancer cells. *J Nanopart Res*. 2018;20(11):300. doi:10.1007/s11051-018-4418-9
40. Zhao H, Duan J, Xiao Y, et al. Microenvironment-driven cascaded responsive hybrid carbon dots as a multifunctional theranostic nanoplatform for imaging-traceable gene precise delivery. *Chem Mater*. 2018;30(10):3438–3453. doi:10.1021/acs.chemmater.8b01011
41. Mulens-Arias V, Nicolás-Boluda A, Gehanno A, Balfourier A, Carn F, Gazeau F. Polyethyleneimine-assisted one-pot synthesis of quasi-fractal plasmonic gold nanocomposites as a photothermal theranostic agent. *Nanoscale*. 2019;11(7):3344–3359. doi:10.1039/c8nr09849b
42. Kumawat MK, Thakur M, Bahadur R, et al. Preparation of graphene oxide-graphene quantum dots hybrid and its application in cancer theranostics. *Mater Sci Eng C*. 2019;103:109774. doi:10.1016/j.msec.2019.109774
43. Sun N, Zhao L, Zhu J, et al. ^{131}I-labeled polyethylenimine-entrapped gold nanoparticles for targeted tumor SPECT/CT imaging and radionuclide therapy. *Int J Nanomed*. 2019;14:4367–4381. doi:10.2147/ijn.s203259
44. Zhao L, Li Y, Zhu J, et al. Chlorotoxin peptide-functionalized polyethylenimine-entrapped gold nanoparticles for glioma SPECT/CT imaging and radionuclide therapy. *J Nanobiotechnol*. 2019;17(1):30. doi:10.1186/s12951-019-0462-6
45. Zheng X, Zhang F, Zhao Y, et al. Self-assembled dual fluorescence nanoparticles for CD44-targeted delivery of anti-miR-27a in liver cancer theranostics. *Theranostics*. 2018;8(14):3808–3823. doi:10.7150/thno.25255
46. Luo X, Peng X, Hou J, Wu S, Shen J, Wang L. Folic acid-functionalized polyethylenimine superparamagnetic iron oxide nanoparticles as theranostic agents for magnetic resonance imaging and PD-L1 siRNA delivery for gastric cancer. *Int J Nanomed*. 2017;12:5331–5343. doi:10.2147/ijn.s137245

47. Gao N, Yang W, Nie H, et al. Turn-on theranostic fluorescent nanoprobe by electrostatic self-assembly of carbon dots with doxorubicin for targeted cancer cell imaging, in vivo hyaluronidase analysis, and targeted drug delivery. *Biosens Bioelectron*. 2017;96:300–307. doi:10.1016/j.bios.2017.05.019
48. Miranda OR, Chen H-T, You CC, et al. Enzyme-amplified array sensing of proteins in solution and in biofluids. *J Am Chem Soc*. 2010;132(14):5285–5289. doi:10.1021/ja1006756
49. Zhou B, Zhao L, Shen M, Zhao J, Shi X. A multifunctional polyethylenimine-based nanoplatform for targeted anticancer drug delivery to tumors in vivo. *J Mater Chem B*. 2017;5(8):1542–1550. doi:10.1039/c6tb02620f
50. Chen C, Zhou B, Zhu X, Shen M, Shi X. Branched polyethyleneimine modified with hyaluronic acid via a PEG spacer for targeted anticancer drug delivery. *RSC Adv*. 2016;6(11):9232–9239. doi:10.1039/c5ra23022e
51. Zhu J, Li H, Xiong Z, et al. Polyethyleneimine-coated manganese oxide nanoparticles for targeted tumor PET/MR imaging. *ACS Appl Mater Interfaces*. 2018;10(41):34954–34964. doi:10.1021/acsami.8b12355
52. Zhu JY, Zhao LZ, Cheng YJ, et al. Radionuclide ^{131}I-labeled multifunctional dendrimers for targeted SPECT imaging and radiotherapy of tumors. *Nanoscale*. 2015;7(43):18169–18178. doi:10.1039/c5nr05585g
53. Zhu JY, Xiong ZJ, Shen MW, Shi XY. Encapsulation of doxorubicin within multifunctional gadolinium-loaded dendrimer nanocomplexes for targeted theranostics of cancer cells. *RSC Adv*. 2015;5(38):30286–30296. doi:10.1039/c5ra01215e
54. Zhu JY, Fu FF, Xiong ZJ, Shen MW, Shi XY. Dendrimer-entrapped gold nanoparticles modified with RGD peptide and alpha-tocopheryl succinate enable targeted theranostics of cancer cells. *Colloids Surf B*. 2015;133:36–42. doi:10.1016/j.colsurfb.2015.05.040
55. Zhu J, Zhao L, Zhao P, Yang J, Shi J, Zhao J. Charge-conversional polyethylenimine-entrapped gold nanoparticles with ^{131}I-labeling for enhanced dual mode SPECT/CT imaging and radiotherapy of tumors. *Biomater Sci*. 2020;8(14):3956–3965. doi:10.1039/d0bm00649a
56. Luong D, Kesharwani P, Deshmukh R, et al. PEGylated PAMAM dendrimers: enhancing efficacy and mitigating toxicity for effective anticancer drug and gene delivery. *Acta Biomater*. 2016;43:14–29. doi:10.1016/j.actbio.2016.07.015
57. Suk JS, Xu Q, Kim N, Hanes J, Ensign LM. PEGylation as a strategy for improving nanoparticle-based drug and gene delivery. *Adv Drug Delivery Rev*. 2016;99:28–51. doi:10.1016/j.addr.2015.09.012